SCIENTIFIC CULTURE
www.sci-cult.com

SCIENTIFIC CULTURE, Vol. 11, No. 1, (2025), pp. 45-61
Open Access. Online & Print

DOI: 10.5281/zenodo.14511048

AN ASSESSMENT OF THE EFFICACY OF ARTIFICIAL AGING METHODS ON THE PHYSICAL AND MECHANICAL CHARACTERISTICS OF STUCCO IN CULTURAL HERITAGE STRUCTURES TREATED WITH ZEOLITE/G-C3N4 HYBRID NANOCOMPOSITES INCORPORATED IN B72/B44 MATRIX

Mohammed Soliman Aly Khedr[1], Mona Foad Ali[2], Ahmed Nabil Emam[3], Abdullah Mahmoud Kamel[4], Manal Abdel-Monem Ghanam[5]

[1]Head of the First Aid Lab, National Museum of Egyptian Civilization, Ministry of Antiquities Conservation Department, Faculty of Archaeology, Cairo University, Giza, Egypt
[2]Faculty of Archaeology, Cairo University, Giza, Egypt
[3]Refractories, Ceramic and Building Materials, Department - National Research Centre (NRC), Dokki, Cairo, Egypt
[4]Faculty of Archaeology, Cairo University, Giza, Egypt
[5]Department of, Egypt Ministry of Tourism and Antiquities, Cairo, Egypt

Received: 15/09/2024
Accepted: 20/12/2024
Corresponding author: Mohammed Soliman Aly Khedr (mohamed.soliman@nmec.gov.eg)

ABSTRACT

Stucco monuments are exceptionally vulnerable to deterioration and necessitate the expertise of specialists in restoration. The current study evaluated the consolidation efficacy of zeolite/g-C_3N_4-based hybrid nanocomposites embedding into a polymeric matrix based on paraloide (B-72-44) in acetone used to treat stucco monuments subjected to damage and distortion after artificial ageing. Zeolite nanoparticles and graphitic carbon nitride nanosheets were prepared via ball-milling and thermal decomposition techniques. In addition, their physicochemical and morphological properties have been investigated using a transmission electron microscope (TEM), X-ray diffraction (XRD), and Fourier transform infrared (FT-IR). After consolidating ageing procedures, the evaluation protocol delineated a six-step procedure to evaluate the suitability of control samples reinforced with the as-prepared zeolite/g-C_3N_4-based hybrid nanocomposites. Also, the alterations in the surface properties of reinforced samples after exposure to diverse conditions have been investigated via digital light and scanning electron microscopy techniques. A colorimeter was employed to quantify the alteration in hue, and assessments were conducted on pre and post-ageing samples. Finally, the determination of physical and mechanical properties and the contact angle are assessed to quantify the hydrophobicity rate. The results showed that zeolite/g-C_3N_4 hybrid nanocomposites are embedded in the B72/B44 matrix. The compositions of Zeolite/g-C_3N_4/B72 and Zeolite/g-C_3N_4/B44 hybrid nanocomposites with 0.5:1:3 wt./wt.% ratio was the most effective for strengthening stucco monuments.

KEYWORDS: Stucco, hybrid nanocomposites, zeolite, graphitic carbon nitride, artificial aging, physical and mechanical properties, color change, contact Angle.

Copyright: © 2025. This is an open-access article distributed under the terms of the Creative Commons Attribution License. (https://creativecommons.org/licenses/by/4.0/).

1. INTRODUCTION

Stucco monuments, a historical artistic expression, are constantly at risk of degradation due to chemical and biological factors (Bloom and Blair, 2009; Caroselli et al., 2020; Bhatnagar, et al., 2010). The hygroscopic and highly porous nature of stucco allows for rapid water circulation, accelerating the process of change and deterioration (Caroselli, Ruffolo, and Piqué, 2021; Oguchi and Yu, 2013; Caratelli, et al.,2013; Treccozzi, et al., 2020). Humidity is a significant and hazardous factor leading to the deterioration of stucco monuments, as it is the primary catalyst for other damaging factors such as biological damage and salts (Cedillo Alvarez, 1987; Sansonetti, et al., 2010; Gulotta, et al., 2012; Zia-ur-Rehman, et al., 2017). Stucco often experiences faults and failures such as structural changes, disintegration, decreased cohesiveness of surface layers, spalling from the substrate, creating bumps, cracks, and color changes (Kroftová and Čejka, 2020; Girsa, and Michoinová, 2013; Mahmou, Kamel and khedr, 2024; England, 2012). Zeolites, microporous aluminosilicate minerals with high surface area, molecular sieving, and ion exchange capacity, are crucial for preserving cultural heritage. They serve as road consolidates, protective layers, and deacidification agents in paper-based artifacts. Their innovative properties and harmless direction make them efficient tools for enhancing the aural integrity of various cultural heritage items (Cruz, et al., 2004). Zeolite nanoparticles, with their high specific surface, small size, and unique ion-exchange and adsorption properties, aid in the preservation of cultural heritage materials. They penetrate porous surfaces of stone, wood, and paper artifacts, forming stable connections that improve their mechanical properties and shield them from environmental threats. Zeolite nanoparticles can neutralize acids and remove harmful substances from paper-based materials, retarding degradation. While zeolite nanoparticles offer potential for cultural heritage conservation, their long-term reliability and security should be considered (Zhang, et al., 2020; Zhang, et al., 2021; Roshen, and Mohsen, 2024; Dedecker, et al., 2018)

Also, graphite carbon nitride (g-C_3N_4) nanoparticles are artificially produced polymers that have electron-rich characteristics, basic surface functions, and H-bonding patterns. These qualities make them a promising candidate to substitute carbon in various material applications (Ezhumalai et al., 2022). These materials are appealing as photocatalysts because they are sensitive to visible light, resistant to photo corrosion and oxidation, chemically stable, have low toxicity to humans, and can alter their optical properties (Lam et al., 2016; He, 2015).

Although g-C_3N_4 has several benefits, it demonstrates limited photocatalytic activity as a result of its poor absorption of visible light, a small specific surface area, and a rapid charge recombination rate. However, there is a lack of consensus on how the structure and composition of g-C_3N_4 impact its ability to kill bacteria. This makes it difficult to prioritize the design of g-C_3N_4 materials for specific performance objectives (Talreja et al., 2023).

The choice of materials for strengthening and adhesive purposes is crucial in cultural heritage preservation. Paraloid, a popular polymeric material used for archaeological materials, has advantages but also has drawbacks, such as poor penetration level (Koob, 1986; Laurenzi and Santamaria, 1985). The physical and mechanical characteristics of acrylic polymers, particularly different forms of paraloid, significantly impact their application in archaeology (Lombardi, 2014). Paraloid B-72 is an advanced material with a lower glass transition temperature, making films softer and having a modest level of reactivity towards sensitive compounds. Paraloid B-44 provides hardness, flexibility, and adherence to substrates, allowing for tailored application formulations (Iezzi, Gaboury, and Wood, 2000). Polymeric nanocomposites, a new type of polymer, have gained attention since the 1990s due to their improved properties compared to individual polymers (Zou, Wu, and Shen, 2008; Wang, et al., 2023; (Verma, et al., 2023, Maria Inês Bruno, et al, 2017). These hybrid nanocomposites, which use various natural and synthetic polymers, have been studied for their potential in stucco monuments preservation. These innovative materials embed different nanomaterials into biopolymers and plastics, enhancing their properties. The addition of nanoparticles, potentially made of one or more nanomaterials, also enhances the matrix's physical, chemical, thermal, and other characteristics (Azadi, Parsimehr and Ershad-Langroudi, 2020; Charkhi et al., 2010). Due to the significance of nanocomposite compounds, it was utilized as the optimal gap-filling paste for antique pottery, comprising a blend of grog, microballoons, and primitive AC33/nano-silica nanocomposites (Mohamed and Mohamed, 2023). Sodium silicate nanoadsorbent is an optimal adsorbent for dye removal and may also be applicable in many environmental research domains (Eslami et al., 2018). As far as we know, no research has been done to assess the performance of hybrid nanocomposites made of zeolite mixed with parolide (B72/B44) and graphite carbon nitride (g-C_3N_4) in acetone. Prior studies have shown that these samples may experience harm or alteration with industrial aging. The work involved the preparation of zeolite and graphitic carbon nitride

nanosheets using ball milling and thermal breakdown chemical techniques. Analytical methods, such as X-ray diffraction (XRD) and Fourier transform infrared (FT-IR), were employed to examine the physical and chemical characteristics of the hybrid nanocomposites. In addition, dynamic light scattering is employed to examine the colloidal characteristics. A six-step approach was devised to assess the appropriateness of standard samples enhanced with nanocomposites following exposure to aging procedures. The evaluation technique entails examining the alterations in the reinforced samples following exposure to different environmental conditions using digital microscopes and scanning electron microscopy (SEM). We evaluated the visual aspect of the samples following the addition of the nanocomposites and subsequent aging. In addition, we utilized a colorimeter to quantify color alterations and conducted a comparative analysis of samples before and following the aging process. Ultimately, the hydrophobicity rate was evaluated by measuring the physical and mechanical properties and the contact angle.

2. METHODS AND MATERIALS

2.1 Methods

USB digital microscopes

Some samples of standard were examined using a portable digital microscope with a magnification ratio starting from 1000X to 500X with the aim of examining and studying the morphological features of the samples. The digital microscope (model PZ01, made by Shenzhen Supereyes co. Ltd., China).

Scanning electron microscopy (SEM)

Some samples of the standard were examined using a SEM Model Quanta 250 FEG (Field Emission Gun) attached to an EDX Unit with an accelerating voltage of 30 KV, a magnification of 14x up to 1000000, and a resolution of 1 nm. FEI Company, Netherlands, at the Grand Egyptian Museum, It is a very useful tool for evaluating the efficiency of reinforcement materials, the depth of penetration, the ability of the material to spread, and the extent of bonding between the material and the treated surface (De Buergo et al., 2004), as well as for characterizing the surface of experimental samples before and after treatment with nanocomposites, and also through the use of the dispersed phase of electrons, which examines more deeply than secondary electrons, which helps in evaluating the extent of penetration of reinforcement materials in contrast to routine morphological examination (Lettieri, and Masieri, 2016). A uniform magnification (2000) was used to make comparisons between the experimental samples correctly.

Determination of the Physical Properties

The specimens' physical characteristics were determined using dry and wet weights. Before the testing, the specimens were dried at 105 °C and weighed before being immersed in distilled water for 20 h and weighed again (Ibrahim et al., 2022). The devices of the Housing and Building National Research Centre in Cairo were used. The physical properties were calculated as follows:

The following equation was used to calculate bulk density in g/cm^3:

$$\mathbf{D = W/V}$$

Where: **W** denotes the starting weight in grams and **V** denotes the volume in cm^3.

Using the following equation, the percentage of water absorption (W.A) was determined.

$$\mathbf{W.\ A=\frac{W2-W1}{W1}\times 100} = \%$$

W1 and **W2** are, respectively, the dry and wet weights in grams.

The following equation was used to calculate apparent porosity (A.P) in %:

$$\mathbf{A.\ P=\frac{W2-W1}{V}\times 100} = \%$$

W1 and W2 are the dry and wet weights in grams, respectively, and V is the volume in cm^3 (Hemeda, et al., 2018).

Compressive Strength Measurement

After identifying the physical properties of these samples, they are mechanically tested to determine the extent of resistance of these mixtures to stresses and pressure on them so that the different Deterioration conditions of the applied model are simulate (Shimmin and van Strien, 2018). A pressure resistance device was used, consisting of two parts: an upper part, i.e., the source of pressure, and a lower part on which the sample is placed. Pressure is placed on the sample in the upper part until it shatters, and then the extent of these samples' tolerance to various pressure factors is calculated. The samples were also put through compression tests according to ASTM C170, which is a standard test method for measuring the compressive strength of dimension stone. The devices of the Housing and Building National Research Centre in Cairo were used.

Color alteration measurements

The color change was measured using a device (PCE-XXM20 Farbmessgerat) to identify the extent of the color change in standard samples after being exposed to artificial aging and make a comparison between standard samples before and after artificial aging. According to Italian guidelines, it should not exceed ΔE on 5 (Oleari, 2000).

Wettability measurements

The hydrophobic or hydrophilic properties of the stucco samples were tested before and after artificial aging by measuring the contact angle. This was done to see how well the surface would hold water using deionized water as a liquid probe and a compact video microscope (CVM 130 X). The samples were placed in the designated place, and then 3-microliter drops of water were placed on the surface of the samples using a graduated micropipette. Then a high-resolution image was taken, and finally the contact angles were calculated.

2.2 Materials and methodology

Preparation of Zeolite nanoparticles.

Urea ($CO(NH_2)_2$, 95% and Zeolite were purchased from El-Gomhouria Chemicals, Egypt. Acetone 98% was purchased from El-Nasr Chemicals, Egypt. Zeolite nanoparticles were prepared via a ball-milling process, as previously reported with little modifications (Charkhi et al., 2010; Sarikaya, et al., 2018; Kong, and Tsuru; 2010). Typically, natural clay (i.e. Clinoptilolite) is loaded into zirconia milling balls into a compatible milling container, with a powder-to-bill ratio of 1:20 mass ratio. Then, appropriate solvents, such as water or a mixture of organic solvents, were added to create the dispersed phase. Next, the sealed container is put in a ball mill or planetary ball mill, and high energy shaking at rotation speeds of up to 200-600 rpm goes on for 2-4 h. The as-produced zeolite nanoparticles were collected via centrifugation at 10,000 rpm after milling. Finally, zeolite nanoparticles undergo oven drying at 80-120°C for 10 h.

Preparation of graphitic carbon nitride (g-C_3N_4) nano-sheets.

The synthesis of graphitic carbon nitride (g-C_3N_4) was carried out through a thermally induced copolymerization process, utilizing urea as the precursor material, following previously reported methods (Wang, et al., 2018, 2020)

In a typical procedure, 100 g of urea were placed in a crucible with a loosely fitted lid. The crucible was then heated in a muffle furnace at a ramping rate of 10 °C/min until reaching a temperature of 550°C. Once the temperature of 550 °C was attained, the crucible was maintained at this temperature for a duration of 4 h. After the 4 h dwell time, the furnace was cooled down to room temperature. Upon cooling, the solid product obtained in the crucible was pristine g-C_3N_4, which was subsequently ground into a fine powder for further usage and applications.

Preparation of Zeolite/g-C_3N_4 – B72- B44 hybrid nanocomposites.

Zeolite/g-C_3N_4 hybrid nanocomposites embedded into B72-B44 polymeric matrix have been fabricated via physical mixing under vigorous high energy ultra-sonication, as follows; the ratio of Zeolite/g-C_3N_4 (Z/g-C_3N_4) was adjusted as reported in Table 1. The as-prepared nano-powders was added to acetone solution of 3 wt/v% of B72-B44 polymeric matrix. The mixture was subjected to high energy ultra-sonication with amplitude of 50% for 30 min with pulse interval of 10 s.

Table 1. Composition of as-prepared Z/g-C_3N_4 hybrid nanocomposites

Samples	Hybrid Nanocomposites Composition
I	Z NPs 0.5 wt/wt% + g-C_3N_4 1 wt/wt% + B72 3 wt/v%
I^+	Z NPs 1.0 wt/wt% + g-C_3N_4 1 wt/wt% + B 72 3 wt/v%
I^{++}	Z NPs 3.0 wt/wt% + g-C_3N_4 1 wt/wt% + B 72 3 wt/v%
J	Z NPs 0.5 wt/wt% + g-C_3N_4 1 wt/wt% + B 44 3 wt/v%
J^+	Z NPs 1.0 wt/wt% + g-C3N4 1 wt/wt% + B 44 3 wt/v%
J^{++}	Z NPs 3.0 wt/wt% + g-C_3N_4 1 wt/wt% + B 44 3 wt/v%

Characterization

The crystallographic properties for each of zeolite nanoparticles and graphitic carbon nitride (g-C_3N_4) nanosheets was carried out using a X'Pert Bruker D8 Advanced X-ray diffractometer (XRD) was employed. The size distribution and zeta potential measurements were performed using a Malvern Zetasizer Nano ZS instrument equipped with a He/Ne laser (wavelength = 633 nm) and backscatter optics at a detection angle of 173°. Furthermore, the Fourier-transform infrared (FT-IR) spectra of the Zeolite and g-C_3N_4 nanoparticles were obtained in the range of 400 to 4000 cm^{-1} using a JASCO 6700 FT-IR spectrometer.

Sample Preparation

The experimental samples, after undergoing tests and analyses on the plaster mask, were investigated according to previous reports on a stucco mask from the National Museum of Ancient Egyptian Civilization (NMEC) (Khedr, et al., 2024). In this case, the experimental samples were prepared to resemble the components of the stucco artifact. The mixture ingredients consisted of hemihydrate (68.2 parts), hydrated

lime (7.2 parts), quartz (sand grains) (3 parts), and dolomite (5.25 parts). The experiment samples were made with dimensions of 3x3x3 cm^3 (ASTM C97/C97M, 2015) and categorized into two groups, A and F, with 9 samples in each group, as shown in Table 2. These test samples were subjected to several artificial weathering cycles, including humidity, drying, and weathering cycles with sodium chloride salt, as shown in Fig. 1. After exposure to different artificial weathering cycles, the experimental samples were evaluated. To assess the suitability of the samples, a six-step protocol was established to determine the level of loss occurring on the samples after exposure to various conditions. This protocol involved the use of a USB digital microscope, a scanning electron microscope (SEM), color change measurements, determination of physical and mechanical properties, and contact angle measurements. These methods were employed to establish standard criteria before and after the samples were subjected to industrial aging processes.

Figure 1. The experimental samples in industrial weathering cycles, where points (A) show the experimental samples before artificial aging, points (B-C) show the experimental samples during different industrial weathering cycles, and point (D) show the experimental samples after industrial Artificial aging.

Mechanical cleaning techniques, including the use of scalpers, scalpels, various brushes, and distilled water, were employed on the experimental samples to remove and extract some of the salt calcifications that had formed during the industrial aging cycles, as shown in Fig. 2. This cleaning process was carried out to prepare the experimental samples for the subsequent stages of the process. The reinforcement of the samples with the as-prepared hybrid nanocomposites, as previously mentioned in Table 1, was then performed to simulate the effect under study. Following this step, a general appearance examination was conducted, where the samples were cleaned with a cloth and visually inspected with the naked eye to ensure that the surface was clean, smooth, and level, free from any imperfections such as bumps, cracks, dimpling, numbness, peeling, or separation.

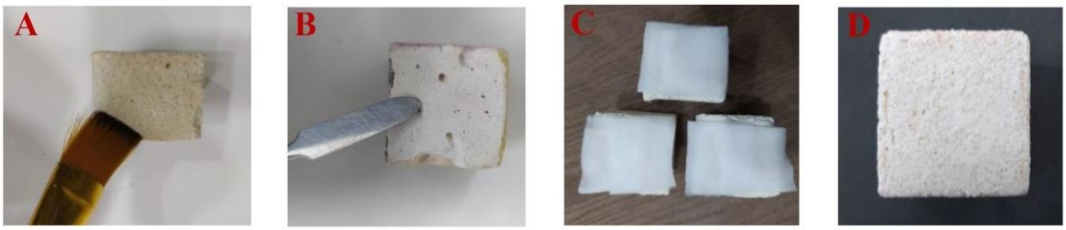

Figure 2. The experimental samples in the mechanical cleaning stages. Point (A) shows the use of brushes, Point (B) Shows the use of scalpels to remove salt calcifications, Point (C) compresses to extract salts, and Point (D) shows the samples after the mechanical cleaning stages.

Upon the application with the Z/g-C_3N_4 hybrid nanocomposites with its different concentrations to the experimental samples, various artificial weathering cycles were carried out [Wang, et al., 2009], as follows:

Humidity-Drying Cycles. The samples were dried before the start of the test at 105°C until the weight was stable, then the samples were weighed, as illustrated in Tables 2 and 3, respectively. Then the treated samples were immersed in water for 4 h, then dried in a closed oven at a temperature of 60° (± 15°) for 18 h. This is followed by leaving the samples in the room atmosphere for 4 hours in order to stabilize them. These steps are repeated for 10 cycles, and the weights are followed up after each cycle and the weights are recorded accurately.

Cycles of weathering with sodium chloride salt. On the same samples, salt cycles were performed followed by drying before the start of the test at 105°C until the weight was stable, then the samples were weighed (Table 2). Then samples were immersed in a 10% solution of sodium chloride salt in water for 3 h. The samples were then dried in a closed oven at a temperature of 60 ± 15 °C for 16 ± 2 h. The samples were then placed in a room atmosphere for 3 hours, and these steps were repeated for 10 cycles. Finally,

the operation of artificial weathering cycles was evaluated, where the average weight and surface changes of the samples were monitored, and comparisons were made for the samples before and after the different stages as well as before and after artificial aging (Group I, Table 2) and (Group J, Table 3)

Table 2. The weight of the experimental samples (Group A) between the different stages and tests.

Samples Stucco before Artificial aging	Weight before drying (g)	Weight after drying(g) 105±2°C	Sample weight After Artificial aging tests before the nanocomposite	Weight after nanocomposite application	Samples after the humidity drying cycles	Samples after the weathering cycles with sodium chloride salt
1I	31.71	28.88	29.76	33.71	33.65	33.12
2I	30.01	27.56	28.77	31.70	31.68	31.07
3I	30.06	27.27	28.19	31.76	31.75	31.19
Average	30.59	27.90	28.90	32.39	32.36	31.79
1I⁺	27.23	25.07	26.38	29.35	29.38	29.11
2I⁺	27.63	25.18	26.87	30.08	29.98	29.65
3I⁺	27.92	25.67	27.04	29.08	29.14	28.58
Average	27.59	25.30	26.76	29.50	29.05	29.11
1I⁺⁺	28.16	25.89	26.88	30.01	30.11	29.76
2I⁺⁺	27.09	24.92	26.12	29.15	29.01	29.08
3I⁺⁺	27.42	25.22	26.87	29.19	29.13	28.87
Average	27.55	25.34	26.62	29.45	29.41	29.23

Table 3. The weight of the experimental samples (Group F) between the different stages and tests.

Samples Stucco before Artificial aging	Weight before drying (g)	Weight after drying(g) 105±2°C	Sample weight After Artificial aging tests before the nanocomposite	Weight after nanocomposite application	Samples after the humidity drying cycles	Samples after the weathering cycles with sodium chloride salt
1J	28.10	25.89	26.88	29.83	29.75	28.99
2J	29.56	27.22	28.13	31.63	31.73	31.04
3J	28.87	26.56	27.58	30.50	30.54	29.68
Average	28.84	26.55	27.53	30.65	30.67	29.90
1J⁺	26.38	24.26	25.18	27.90	27.82	26.87
2J⁺	26.59	24.47	25.51	28.31	28.12	27.56
3J⁺	27.83	25.67	26.58	29.80	29.35	27.98
Average	26.93	24.80	25.75	28.76	28.49	27.47
1J⁺⁺	26.20	24.12	25.21	27.71	27.62	25.65
2J⁺⁺	29.67	27.43	28.39	31.74	31.55	30.17
3J⁺⁺	26.89	24.80	26.01	28.39	28.24	27.45
Average	27.58	25.45	26.53	29.28	29.13	27.75

3. RESULTS AND DISCUSSION

Preparation and characterization of Zeolite/g-C_3N_4 hybrid nanocomposites

The XRD patterns of virgin g-C_3N_4, as shown in Fig. 3a, revealed two distinct peaks at approximately 13.1° and 27.4°, which are consistent with the crystalline structures of g-C_3N_4 [Zhang, et al., 2021]. The high-intensity peak at 27.4° corresponded to an interlayer distance of 0.326 nm and was attributed to the aromatic segment stacking, identified as the (002) peak typically observed in graphitic materials. The low-intensity peak at 13.1°, with an interlayer spacing of 0.676 nm, was assigned as the (100) peak and could be linked to the in-plane structural packing motif of tri-s-triazine units [38, 49].

Additionally, Fourier-transform infrared (FTIR) spectroscopy was employed to analyze the functional groups present in the as-prepared g-C3N4 samples, and the results are depicted in Fig. 3b. The typical spectra of each sample exhibited similar features. The intense bands in the region of 1200-1700 cm^{-1} corresponded to the stretching vibration modes of aromatic CN heterocycle repeating units (Wang, et al., 2018; Bojdys, et al., 2008). The triazine (C_3N_3) units typically exhibited a band around 800 cm^-1, indicating their breathing mode. The peaks in the range of 3100-3400 cm^{-1} were attributed to the stretching vibration of a minor amount of residual amino (-NH_2) groups [Wang, et al., 2018, Zheng, et al., 2016].

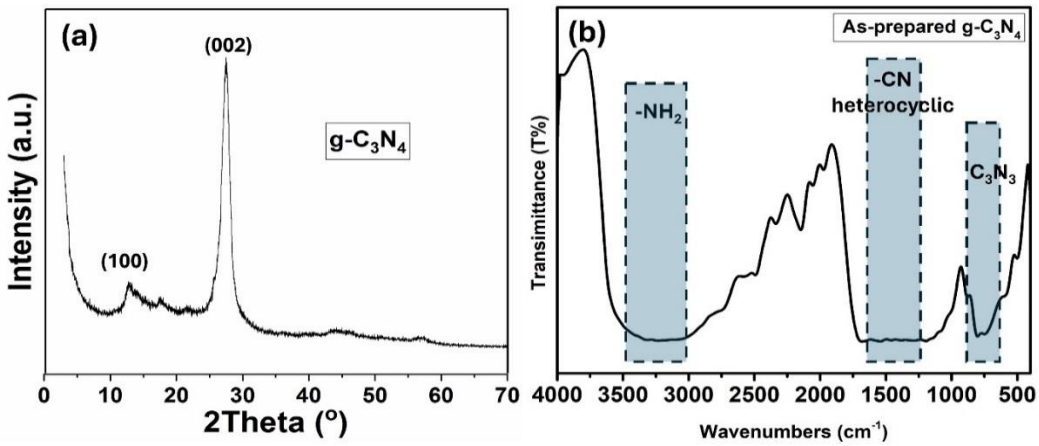

Figure 3. XRD patterns (a) and FT-IR spectra (b) of as-prepared g-C_3N_4 nanosheets

Furthermore, the colloidal properties, such as hydrodynamic diameter (H_D) and zeta potential (ζ), were determined using the dynamic light scattering (DLS) technique. As shown in Fig. 4, the hydrodynamic diameter (H_D) was approximately 290 ± 33.76 nm, and the polydispersity index (PDI) was around 1.00 (See Fig. 4a). Additionally, the zeta potential (ζ, mV) exhibited a moderate stability of about -14.8 mV, as illustrated in Fig. 4b.

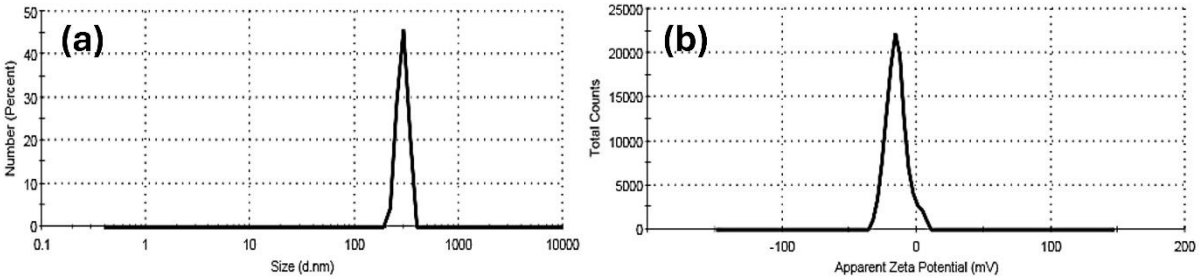

Figure 4. DLS (a) and Zeta-potential (b) of as-prepared g-C_3N_4 nanosheets

The crystallographic structure of zeolite nanoparticles has shown five main distinct features at two theta (2θ) of 9.875, 19.07, 22.46, 28.13 and 30.05 ° that corresponding to (0 2 0), (1 3 -1), (4 0 0), (4 2 -2) and (1 5 1) reflections, respectively, indicated to a crystalline with monoclinic structure (C2/m) as illustrated in Fig. 5. Finally, the colloidal properties based on the particle size distributions and zeta potential for zeolite NPs are shown in Fig. 6. While the hydrodynamic diameter (H_D) was about 122.3 ± 21.11 nm with a polydispersity index (PDI) of 0.614. Also, zeolite NPs showed a low stability dispersion with a zeta potential of -8.36 mV.

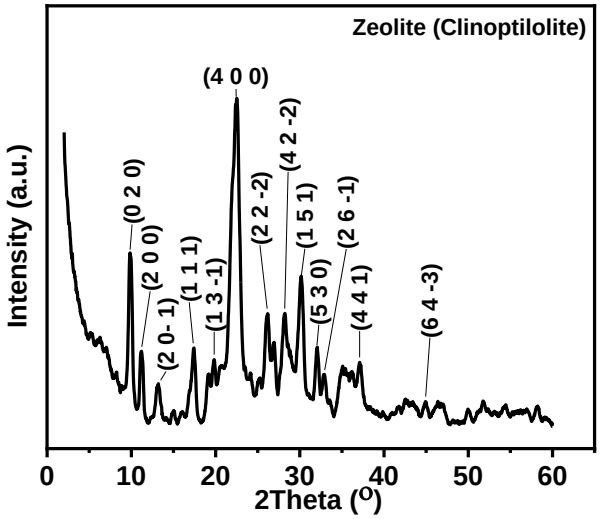

Figure 5. XRD patterns of zeolite NPs

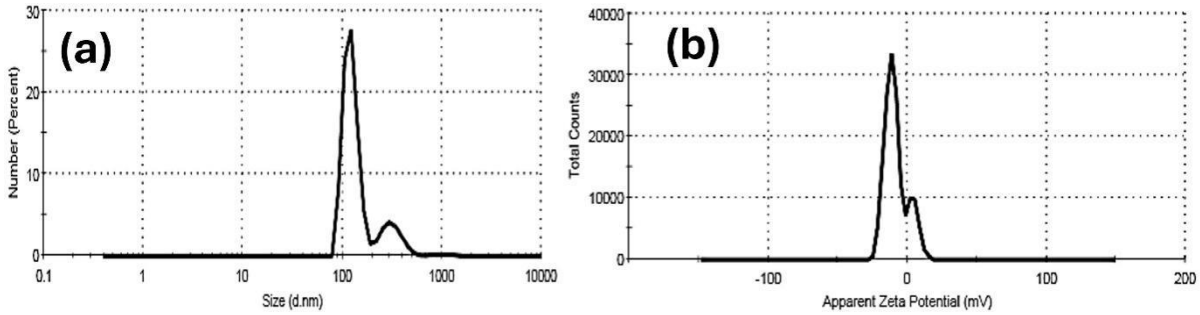

Figure 6. DLS (a) and Zeta-potential (b) of as-prepared zeolite nanoparticles

Fig. 7 illustrates the results of group (I) following the application of the nanocomposite, the humidity-drying cycles, and the sodium chloride salt weathering cycles as follows: A mass variation occurred in the experimental samples, as shown in Table 2. The researchers conducted a thorough investigation using a digital camera and USB microscope upon application of the nanocomposite. This examination confirmed the presence of blocked pores and air gaps, as well as the absence of fractures, pits, and cohesiveness in certain fragmented areas, as indicated by points (1, 2, 3). We observed a conspicuous layer with slight cracks on the surface of the experimental samples (Group, I^{++}). This was clearly visible under a USB microscope at a magnification of 500X, as depicted in point 4. After conducting the fake aging experiments, we found a noticeable alteration in hue, as specified in point 5. Point 6 indicates that we observed evident signs of minor surface pitting and cracks in Group (I-I^{+}), particularly following the second test. The experimental materials in Group I^{++} exhibited evident signs of damage, including loss, pitting, fragmentation, and thick cracks, particularly after the second test, as indicated by points (7, 8).

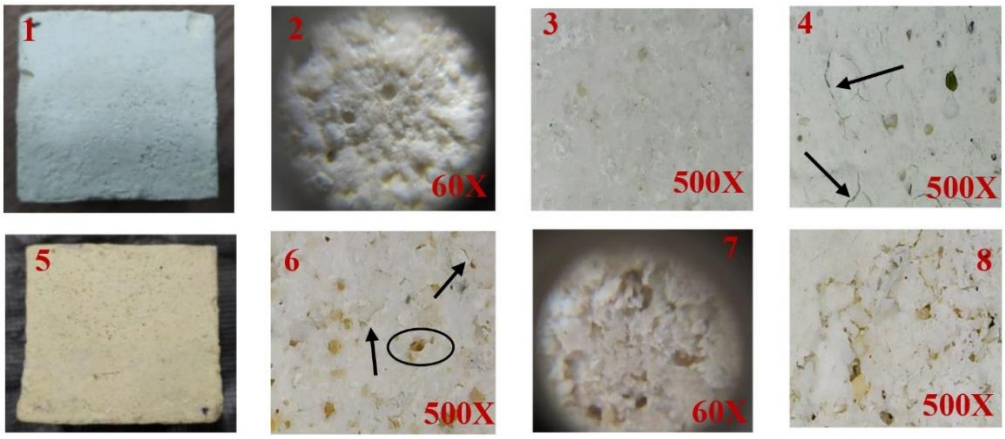

Figure 7. The results of group (I) after applying the nanocomposite, after wet-drying cycles, and after weathering cycles with sodium chloride salt.

Fig. 8 depicts group I's outcomes after the implementation of the nanocomposite, the humidity-drying cycles, and the weathering cycles with sodium chloride salt. The arrows shown in the picture indicate the cracks and salts that appeared on the samples after aging.

As shown in Table 3, the weight of the experimental samples changed. The researchers conducted a comprehensive analysis of the nanocomposite using a digital camera and USB microscope, which revealed the effective obstruction of pores and air gaps. Furthermore, certain fragmented components exhibited no signs of cracks, pits, or lack of cohesiveness. Additionally, the researchers made distinct observations regarding the transparency and visual characteristics of the surface and its grains, as outlined in points (1, 2, 3). The researchers observed that the experimental samples exhibited a depletion of surface layers, resulting in a high level of transparency. The surface grains were clearly visible through a 500X USB microscope, as demonstrated in point 4. Following the fake aging experiments, the researchers noted a discernible alteration in hue. As stated in point 5, also saw a depletion of layers. Notably, salts appeared on the surface and inside the gaps and pores, causing layers to erode, particularly those strengthened by nanocomposites. This became more apparent following the second exam, as evidenced by points (6, 7, 8).

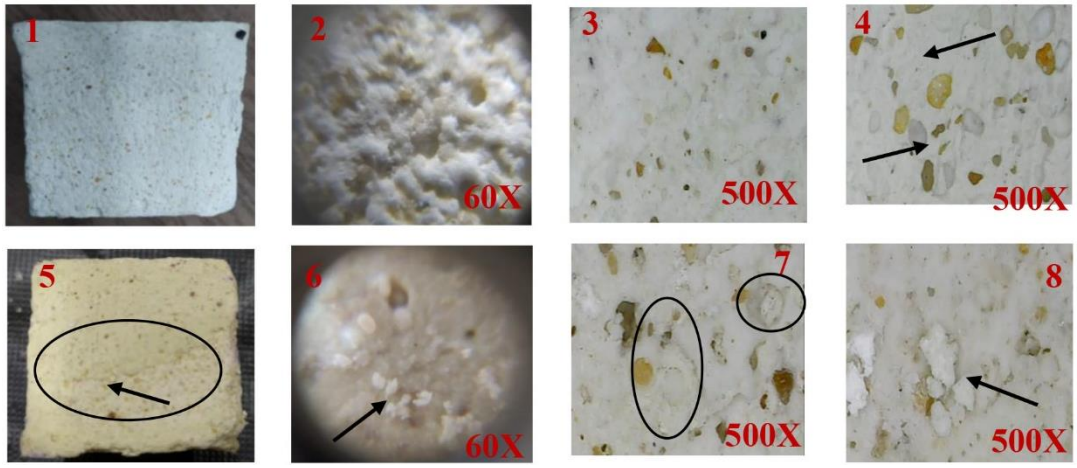

Figure 8. The results of group (J) after applying the nanocomposite, after wet-drying cycles, and after weathering cycles with sodium chloride salt.

The evaluation of the effectiveness of Zeolite/g-C3N4 hybrid nanocomposites embedded in B72-B44 matrix has been conducted on the test samples belonging to groups (I, J). The evaluation entailed developing a six-step procedure to assess the appropriateness of the reinforcement materials on the experimental samples.

Weight loss in the experimental sample group (I, J)

Upon comparing the average loss following the compound and Artificial aging tests, as presented in Tables 2 and 3, there was a little variation in the average percentages. The group I had the highest level of loss, with a value of 0.60. The group I+ experienced a loss percentage of 0.39. The group I++ experienced a 0.22 loss percentage. The group labelled as (J++) experienced the highest level of loss, with a value of 1.53. The group labelled as (J+) had a loss percentage of 1.29. The group labelled as J performed the best, with a loss value of 0.75.

An examination is conducted using a USB digital microscope, following the specifications of the American ASTM standard. The surfaces of the samples will be compared before and after artificial aging using a digital camera (USB 60X and USB 500X) in group (I, J).

Analysing the results of the virtual or visual inspection and determining the overall appearance, as illustrated in Fig. 9.The observations that are presented in Figure 9 are as follows: Put together (I) It is possible to draw the conclusion that the compound Zeolite/g-C3N4 hybrid nanocomposites contained in the B72 matrix are effective after comparing the experimental samples before and after the application of the nanocomposite, as well as after the application of artificial aging.

The optimal concentration of the compound is 0.5%, 1%, 3%, as demonstrated in experimental samples (I). The compound exhibited a composition of (1%:1%:3%) in the initial experimental samples (I^{+}). However, upon increasing the composition to (3%:1%:3%) in the subsequent experimental samples (I^{++}), the compound experienced damage and developed a surface layer filled with fractures and fissures. This suggests that reducing the percentage of nanocomposite enhances the reinforcing ability of Stucco monuments.

Assemblage (J) After comparing the experimental samples before and after the nanocomposite application, and after artificial aging, we can conclude that the compound Zeolite/g-C3N4 hybrid nanocomposites embedded in the B44 matrix is not suitable. The surface experiences general deformation due to the loss of surface layers and the formation of dense salt deposits. However, group J, with a concentration of 0.5%, 1%, and 3%, saw the lowest amount of loss and deterioration.

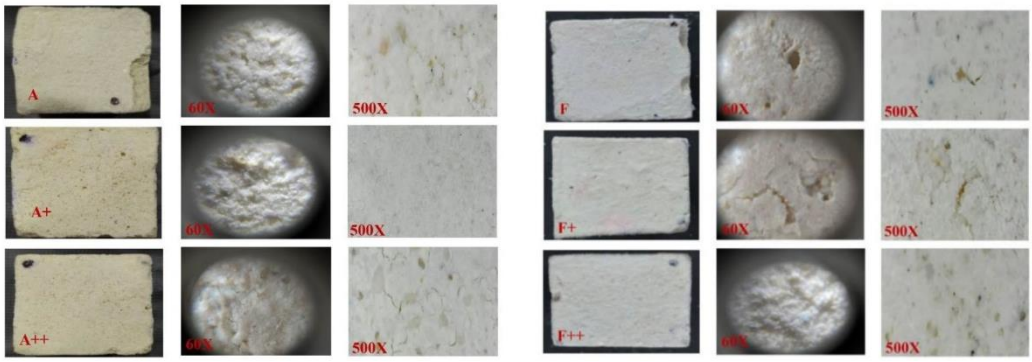

Figure (9) shows the final evaluation of the nanocomposite after artificial aging through visual inspection, group (I, J).

Morphological examination by scanning electron microscope (SEM) and making a comparison between the experimental samples before and after artificial aging, uniform magnification (2000) was used in order to make comparisons between the experimental samples correctly. SEM morphological examination of the experimental samples before applying the nanocomposite and after artificial aging, as shown in Figure (10), points (1-2), and in comparison, between the experimental samples after applying the three concentrations of the nanocomposite and also after artificial aging.

SEM (group I): The results of the SEM analysis corroborate those of the visual analysis. Experimental samples (I) show surface stability at the lowest concentration (0.5%: 1%: 3%), while experimental samples (I^{+}) show stability at higher concentrations (1%: 1%: 3%), both of which are validated by SEM analysis. However, the compound was degraded and a thick layer with numerous cracks and crevices was formed on the surface when the percentage climbed to (3%: 1%: 3%), as demonstrated in the testing samples (I^{++}). Additionally, by contrasting the experimental samples taken before and after artificial aging, we find that the samples taken after aging (I) retain their cohesiveness and do not include any fissures, breaks, or gaps between their atoms. A few surface salts and few simple interatomic gaps were detected in the I+ test samples. The experimental samples (I^{++}) exhibited a generalized surface deterioration and an increase in surface salt percentages, as illustrated in Fig.10.

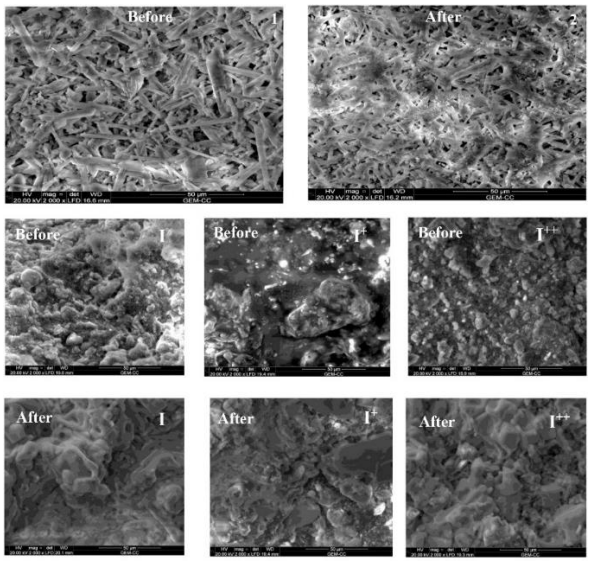

Figure 10. group (I). shows a contrast between normal samples before and after Artificial aging (points 1-2), as well as between samples before and after using the nanocomposite and after Artificial aging them artificially using an SEM.

SEM (group J): To back up what the visual analysis showed, the SEM analysis results show that the surface stays stable at the lowest concentrations (0.5%, 1%, and 3%), as shown in the experimental samples (I). Nevertheless, the experimental samples (I^{+}) revealed a slight degradation at concentrations of 1%, 1%, and 3%. However, upon increasing the percentage to 3%, 1%, and 3%, the compound experienced degradation, forming a thick layer filled with numerous cracks and crevices. Since the loss of surface layers and the build-up of salts on the surface caused the surface to change shape all over, we can

say that the Zeolite/g-C3N4 hybrid nanocomposites embedded in B44 matrix is not a good compound for comparing samples before, after, and after artificial aging. On the other hand, group J concentration (0.5%, 1%, and 3% by weight) caused the least amount of loss and degradation. as illustrated in Fig. 11.

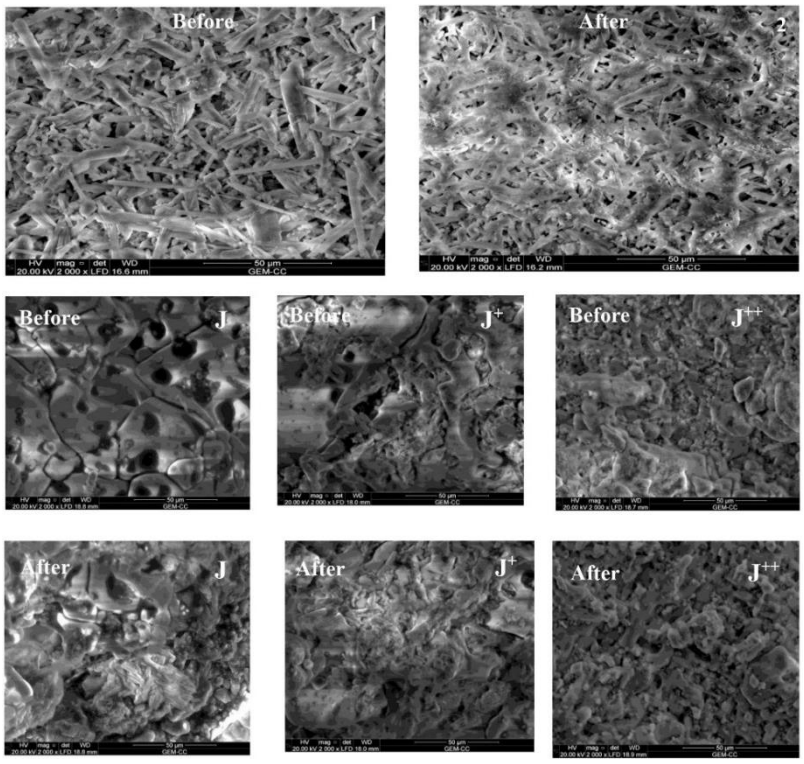

Figure 11. group (J). shows a contrast between normal samples before and after Artificial aging (points 1-2), as well as between samples before and after using the nanocomposite and after Artificial aging them artificially using an SEM.

Colour alteration measurements

A color alteration test was carried out to evaluate the differences between the experimental samples, as shown in Tables (4-5) After treatment and strengthening with nanocomposites and after studying industrial Artificial aging, group (I, J). according to the equation below:

$$\Delta E=\sqrt{(\Delta l*)^2+(\Delta a*)^2+(\Delta b*)^2}$$

Colour alteration measurement group (I). When comparing the experimental samples after strengthening with nanocomposites and after industrial Artificial aging, we conclude that a colour change occurred in the experimental samples (I) with an average of (2.76), the experimental samples (I^+) with an average of (1.57), and the experimental samples (I^{++}) with an average of (5.64), We conclude from this that when the proportions of the nanocomposite are low the percentages of colour change decreased, as shown in Table 4.

Table 4. The colour change test for the experimental samples (group I) after strengthening with nanocomposites and after artificial aging.

ΔE	After industrial aging			after strengthening with nanocomposites			group (I)
	L**	a**	b**	L*	a*	b*	
3.11	76.81	-29.86	1.84	80.04	-28.81	5.02	**1I**
4.17	76.80	-31.46	1.91	80.95	-28.40	5.44	**2I**
1.00	79.10	-31.24	2.99	79.84	-29.83	3.57	**3I**
0.77	77.78	-29.88	3.85	77.42	-31.53	3.98	**1I$^+$**
2.72	77.93	-29.20	3.80	81.11	-29.65	6.76	**2I$^+$**
1.24	76.03	-33.22	3.27	76.52	-35.17	3.37	**3I$^+$**
5.83	75.83	-36.67	1.41	80.39	-30.18	6.51	**1I^{++}**
8.10	74.80	-39.46	0.68	84.67	-36.83	7.67	**2I^{++}**
3.01	76.13	-34.72	0.78	77.12	-32.91	5.16	**3I^{++}**

Color alteration measurement group (J). When comparing the experimental samples after strengthening with nanocomposites and after artificial aging, we conclude that a color change occurred in the experimental samples (J) with an average of (1.49), the experimental samples (J^{+}) with an average of (2.95), and the experimental samples (J^{++}) with an average of (5.97). We conclude from this that when the percentages of the compound increased, the percentage of color change increased, as shown in Table 5.

Table 5. The color change test for the experimental samples (group J) after strengthening with nanocomposites and after artificial aging.

ΔE	After industrial aging			after strengthening with nanocomposites			group (J)
	L**	a**	b**	L*	a*	b*	
0.74	79.03	-31.22	3.74	78.19	-32.02	3.50	1J
1.34	79.70	-31.90	3.70	77.90	-32.16	3.02	2J
2.41	79.63	-31.11	3.68	76.76	-28.29	3.63	3J
1.39	76.21	-28.16	2.92	77.13	-31.09	4.38	$1J^{+}$
5.04	76.54	-23.90	2.81	75.16	-34.89	3.71	$2J^{+}$
2.42	77.48	-27.29	3.73	79.29	-32.19	5.53	$3J^{+}$
5.44	74.60	-36.06	3.62	80.74	-29.27	4.51	$1J^{++}$
5.44	75.46	-31.45	3.59	82.27	-26.85	4.86	$2J^{++}$
7.05	73.63	-39.12	2.97	81.04	-29.29	4.55	$3J^{++}$

Determination of the physical and mechanical properties of the experimental samples

Determine the physical properties (water absorption and apparent porosity) and mechanical properties (compressive strength test) of the experimental samples, both before and after artificial aging, for groups I-J. Compare them to the average results of standard samples without any additives that were subjected to aging. The graph (12-13) illustrates the industrial process. The physical and mechanical properties of the samples were compared before and after artificial aging. The compound Zeolite/g-C_3N_4 hybrid nanocomposites embedded in B72 matrix was found to be a good one at concentrations of 0.5%, 1%, and 3%. Group (I). This is because the average water absorption rate of the experimental samples is 19.03 and compared to the standard samples (30.23), and it has decreased by 11.02, and so on in their average porosity (23.33) and compared to the standard samples (36.70), and it decreased by 13.37. So, it had concluded that the percentage decreased and the experimental samples improved in terms of their physical properties. Additionally, the average resistance of the samples to pressure increased to 22.01, compared to 8.89 for the standard samples. This leads to conclude that the percentage has increased. The experimental samples are in better condition in terms of their mechanical properties. We compared the average percentage of water absorption of the experimental samples after artificial aging (22.29) to the samples before aging (19.03), and found a slight increase (3.26). Thus, in their average porosity increased by a slight difference (4.26) compared to the samples before artificial aging. This leads us to conclude that the experimental samples did not sustain significant physical property damage, and their average resistance to pressure decreased by 7.35 after artificial aging (14.66) compared to their pre-aging (22.01) samples. This leads to conclude that the experimental samples lost strength in their mechanical properties, but not in their condition prior to applying the compound, as the standard samples' resistance to pressure before and after aging was 8.89, indicating a significant difference. (5.77). The compound significantly enhanced the physical and mechanical properties of the experimental samples, as evidenced by the fact that they underwent artificial aging twice after applying the compound, compared to just one exposure before. as shown in graph (12).

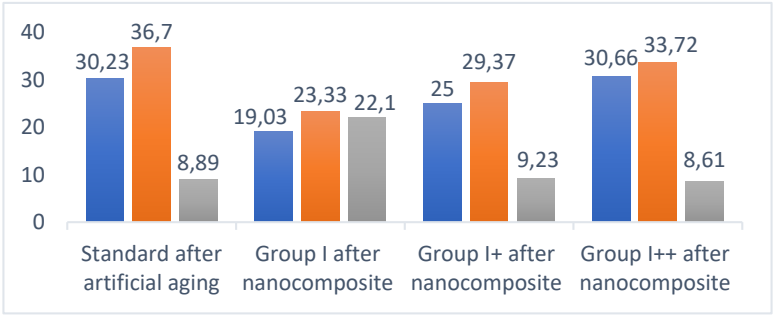

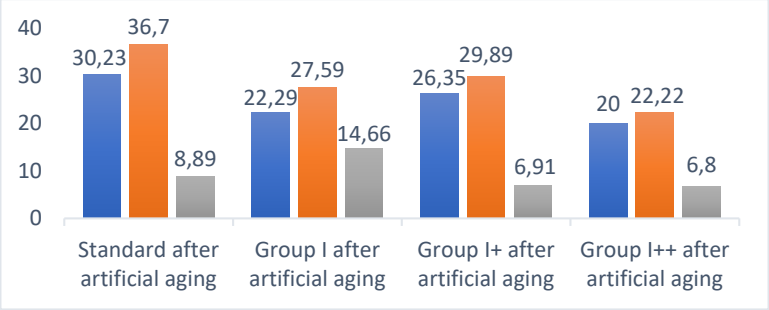

Figure 12. physical properties (water absorption, and apparent porosity) and mechanical (compressive strength test) of the experimental samples. group I.

After discussing the results of determining the physical and mechanical properties of the experimental samples before and after artificial aging, compound Zeolite /g-C_3N_4 hybrid nanocomposites embedded in B44 matrix is a good compound with a concentration of 0.5%, 1%, 3%. Group (J). As for the compound at a concentration of 3%, 1%, 3%, Group (J^{++}) was a good compound before artificial aging, but it deteriorated after artificial aging. As for the compound at a concentration of 1%, 1%, 3%, Group (J^{+}) wasn't a good compound before and after artificial aging, but it deteriorated artificial aging.as shown in in Fig. 13.

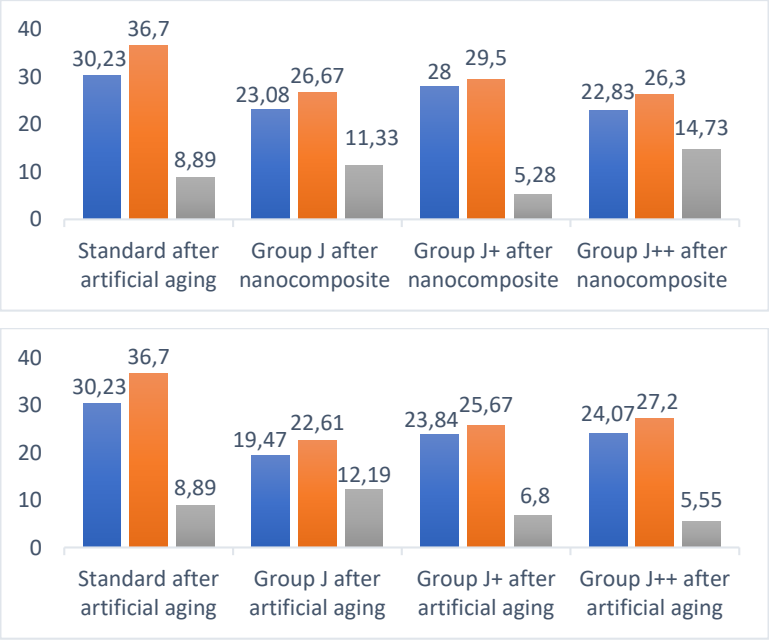

Figure 13. Pphysical properties (water absorption, and apparent porosity) and mechanical (compressive strength test) of the experimental samples group F.

Wettability measurements (Static water contact angle) group I-J

Static water contact angle Group (I): When comparing the rate of hydrophobicity of the nanocomposite between the standard samples and the samples to which the nanocomposite was added, we notice a significant change, as shown in Fig.14, where we notice the following:

1- There was a significant change in the measuring angles between the standard samples before artificial aging (60 ^{o} -69^{o}) and after artificial aging (51^{o} -47^{o}), with a difference of (9^{o} -22^{o}). This shows the extent of deterioration of the samples' surfaces and the rate of their hydrophobicity.

2- When comparing the angle measurements between standard samples after artificial aging (51^{o} -47^{o}), group (I) (110^{o} -111^{o}) with a difference of (59^{o} -64^{o}), group (I^{+}) (102^{o} -101^{o}) with a difference of (51^{o} -54^{o}), and group (I^{++}). (97^{o} -98^{o}) with a difference of (46^{o} -51^{o}). It is clear to us that there is an increase in the rate of hydrophobicity of the samples after applying the compound and before performing the artificial aging work. We conclude that the best is group (I) by a very large difference, followed by group (I^{+}), then after that group (I^{++}).

3- When comparing the angle measurements between the experimental samples before and after aging, it becomes clear to us that group (I) had a change in angles with a difference of (35° -34°), group (I+) with a difference of (30° -30°), and group (I++) with a difference of (31° -33°).We conclude that all groups after artificial aging obsolescence changed at a similar rate.

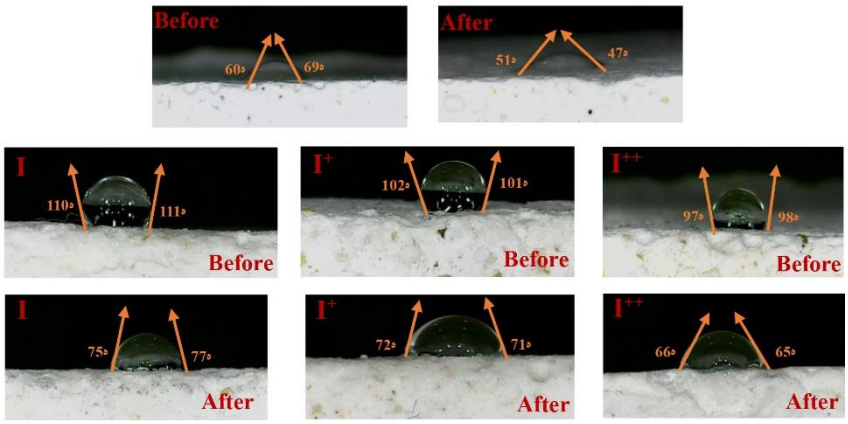

Figure 14. The static water contact angle of Group (I)

Static water contact angle Group (J): When comparing the rate of hydrophobicity of the nanocomposite between the standard samples and the samples to which the nanocomposite was added, we notice a significant change, as shown in figure (15), where we notice the following:

1) There was a significant change in the measuring angles between the standard samples before artificial aging (60° -69°) and after artificial aging (51° -47°), with a difference of (9° -22°). This shows the extent of deterioration of the samples' surfaces and the rate of their hydrophobicity.

2) When comparing the angle measurements between standard samples after aging (51° -47°), group (J) (116° -115°) with a difference of (65° -68°), group (J+) (112° -108°) with a difference of (61° -61°), and group (J++) (102° -99°) with a difference of (51° -52°). It is clear to us that there is an increase in the rate of hydrophobicity of the samples after applying the compound and before performing the artificial aging work. We conclude that the best is group (J), followed by group (J+), and after that group (J++).

3) When comparing the angle measurements between the experimental samples before and after artificial aging, it becomes clear to us that group (J) had a change in angles with a difference of (44° -47°), group (J+) with a difference of (46° -44°), and group (J++) with a difference of (39° -38°). We conclude that all groups after artificial aging obsolescence changed at a similar rate.

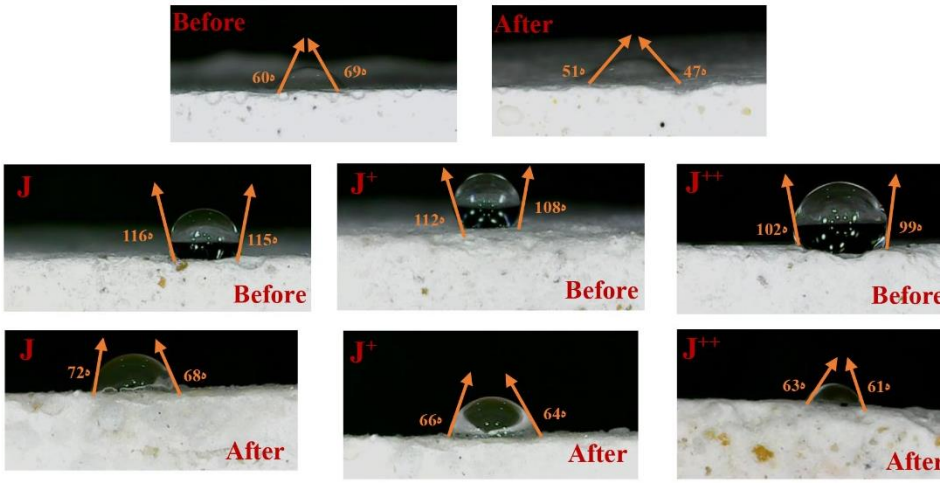

Figure 15. The static water contact angle of Group (J)

4. CONCLUSION

Assessment of the physical and mechanical characteristics of stucco treated with zeolite/g-C_3N_4 hybrid nanocomposites embedded in B72/B44 matrix as a result of artificial ageing procedures concluded. Following the 6-step protocol, we were able to determine that the compound containing 0.5% Zeolite, 1% g-

C_3N_4, and 3% B was the most effective in terms of strengthening, as measured by the weight loss percentage of the experimental samples (0.60%), overall appearance, and morphological examination using an electron microscope. Efficiency, penetration depth, material spreading ability, extent of bonding between the treated surface, rate of hydrophobicity of the nanocomposite (contact angle), and simple color change rate up to 2.76 were the scanner-displayed characteristics that set the composite apart from its competitors when it came to determining physical and mechanical properties.Due to the overall surface deformation caused by the loss of surface layers and the dense formation of salts on the surface, it became evident during the 6-step protocol that the compound Zeolite / g-C_3N_4 hybrid nanocomposites embedded in B44 matrix is not a good compound. However, the concentration of 0.5% Zeolite + 1% g-C_3N_4 + B 44, 3% resulted in the lowest loss and deterioration.

Conflicts of interest

There are no conflicts to declare.

Funding: No Fund

Acknowledgments

We would like to express our heartfelt appreciation to the anonymous reviewers, whose suggestions significantly improved this work.

Authors contribution

M.K. M.A. and A.A. conceived of the presented idea. M.K. developed the theory and performed the computations. M.K and A.K. verified the analytical methods. M.G. and M.A. encouraged M.K. to investigate [a specific aspect] and supervised the findings of this work. All authors discussed the results and contributed to the final manuscript.

REFERENCES

Azadi, N., Parsimehr, H., and Ershad-Langroudi, A. (2020), Cultural heritage protection via hybrid nanocomposite coating, Plastics, *Rubber and Composites,* Vol. 49, No. 9, pp.414-424.

Bhatnagar, P., et al., (2010) *Biodeterioration of archaeological monuments and approach for restoration*, CRC press Science Publishers, Enfield.

Bloom, J. M. and Blair, *S. S.* (2009) *The Grove Encyclopedia of Islamic Art & Architecture: Three-Volume Set*. Oxford University Press, Vol. 1, pp. 1-7.

Bojdys, M.J., Müller, J.O., Antonietti, M., and Thomas, A. (2008) synthesis of crystalline, condensed, graphitic carbon nitride, *Chemistry–A European Journal,* Vol. 14, No. 27, pp. 8177-8182.

Caroselli, M., et al., (2020) *Composition and techniques of the Ticinese stucco decorations from the 16th to the 17th century: results from the analysis of the materials.* Heritage Science, Vol. 8, No. 102, pp. 1-20.

Caroselli, M., Ruffolo, S. A., and Piqué F. (2021). *Mortars and plasters – how to manage mortars and plasters conservation.* A*rchaeological and Anthropological Sciences*, Vol. 13, No.11, pp. 1-20

Caratelli, A., Siani, A., Casale, G., Paravicini, A., Fiore, K., and Dario, D. (2013) Stucco panels of Room VI in the Galleria Borghese (Rome): Physical–chemical analysis and microclimate characterization, *Energy and Buildings*, Vol. 61, pp.133–139.

Corzo, M.A. et al. (1987) *In situ archaeological conservation: proceedings of meetings April 6-13, 1986, Mexico*. [Los Angeles, Calif.], [Mexico City, Mexico]: Getty Conservation Institute ; Instituto Nacional de Antropologia e Historia, Mexico.

Cruz, A.J., et al., (2004) Adsorption of Acetic Acid by Activated Carbons, Zeolites, and Other Adsorbent Materials Related with the Preventive Conservation of Lead Objects in Museum Showcases. *Journal of Chemical & Engineering Data*, Vol. 49, No.3, pp. 725-731.

Čejka, T and Kroftová. *Materials and technologies for the consolidation of historic plasters by the wetting and surface penetration method,* The Civil Engineering Journal, 2020, Vol. 29, No.4, pp.414-424.

Dedecker, K., et al., *(2018)* Metal-Organic Frameworks for Cultural Heritage Preservation: The Case of Acetic Acid Removal, *ACS Applied Materials & Interfaces*, Vol. 10, No.16, pp. 13886-13894.

De Buergo, M. A., Fort, R. and Gómez-Heras M *(2004)* Contributions of scanning electron microscopy to the assessment of the effectiveness of stone conservation treatments. *Scanning: The Journal of Scanning Microscopies,* Vol. 26, No.1, pp. 41-47.

Henry, A. and Stewart, J. (2012) *Practical Building Conservation: Mortars, Plasters and Renders,* Ashgate Publishing, Ltd, pp. 613-2012.

Eslami, A., Mehralian, M., Cheginic, C.Z. and Khashij, M. (2018) Application of nanosilicabased adsorbent for the removal of rhodamine B and methylene blue from aqueous solutions, *Desalination and Water Treatment*, Vol. 108, pp.345-352.

Ezhumalai, Y., Kumaresan, P. and Jayapalan, T. (2022) Graphite Carbon Nitride, Photocatalysts-New Perspectives, IntechOpen.

Fassina, V. (1993) Stone material in monuments: Diagnosis and conservation, Scuola universitaria CUM conservazione dei monumenti). Heraklion, Crete, pp.24-30.

Gulotta, D., Goidanich, S., Bertoldi, M., Bortolotto, S., and Toniolo, L. (2012) "Gildings and False Gildings of the Baroque Age: Characterization and Conservation Problems", *Archaeometry*, Vol. 54, pp. 940–954.

Girsa, V. and Michoinova, D. (2013) *Historické Omítky: Záchrana, Konzervace, Obnova: (metodika přístupu k historickým omítkám a k jejich záchraně)*. vyd. 2. Praha: Ceské Vysoké Učení Technické, ISBN 978-80-87104-99-6.

Hemeda, S., et al., (2018) The effectiveness of nano materials and nanomodified polymers for preservation of historic brick masonry in Rashid, Egypt. *International Journal of Conservation Science,* Vol. 9, No. 4. pp. 835-846.

Jijiang, H. (2015) Preparation and photocatalysis of graphite carbon nitride based photocatalysts, School of Chemical and Petroleum Engineering Department of Chemical Engineering, Curtin University, pp. 1-95.

Khedr, M.S., Aly, M.F., Kamel, A.M., and Elghanam, M. (2024). "Characterization Study of a Roman Stucco Death Mask from the National Museum of Egyptian Civilization, *Egyptian Journal of Chemistry,* Vol. 67, pp. 109-119

Ibrahim, M.M., Mohamed, W. S. and Mohamed H.M. (2022) Evaluation of the efficacy of traditional and nano paraloid b72 for pottery consolidation. *International journal of conservation science,* Vol. 13, No. 1, pp. 15-30.

Kong, C. and Tsuru, T. (2010) Zeolite nanocrystals prepared from zeolite microparticles by a centrifugation-assisted grinding method. *Chemical Engineering and Processing: Process Intensification*, Vol. 49, No. 8, pp. 809-814.

Koob, S.P. (1986) "The use of Paraloid B-72 as an adhesive: its application for archaeological ceramics and other materials", *Studies in conservation*, Vol. 31, pp. 7-14.

Laurenzi, T. M. and Santamaria. U. (1985). Consolidant and protective effects of different products on Lecce limestone. In: *Congrès international sur l'altération et la conservation de la pierre, Vol.5*, pp.697-707.

Lana, R. T. and Mohsen, A. J. (2024) A Review of Nanotechnology in Self-Healing of Ancient and Heritage Buildings: Heritage buildings, Nanomaterial, Nano architecture, Nanotechnology in construction. *International Journal of Nanoelectronics and Materials*, Vol. 17, No.1, pp. 153-163.

Lam, S.M, Sin, J.C. and Mohamed, A.R. (2016) A review on photocatalytic application of g-C3N4/semiconductor (CNS) nanocomposites towards the erasure of dyeing wastewater, *Materials Science in Semiconductor Processing*, Vol. 47, pp. 62-84.

Lettieri, M. and Masieri, M. (2016) Performances ndly Restoration Mortars for Historic Lime-based Stucco and Building Materials. *Periodica Polytechnica Civil Engineering. Composite Materials for High-Efficiency Multiple Protection of Paper Relics.* Industrial & Engineering Chemistry Research, Vol.59, No. 24, pp. 11196-11205.

Lettieri, M. and Masieri, M. (2016). Performances and coating morphology of a siloxane-based hydrophobic product applied in different concentrations on a highly porous stone. *Coatings,* Vol. 6, No. 4, pp. 60.

Iezzi, R. A., Gaboury, S. and Wood, *K.* (2000) Acrylic-fluoropolymer mixtures and their use in coatings. *Progress in organic coatings*, Vol. 40, No. 1-4, pp. 55-60.

Maria Inês Bruno, T., et al., (2017) *Polymer Nanocomposites*, in *Nanostructured Materials*, S. Mohindar Singh, Editor, IntechOpen: Rijeka, pp.7.

Lombardi, E. (2014) Biotechnologies for restoration of cultural heritage. PhD thesis, Università degli studi di Milano

Mohamed, M.G., Ahmed, N.M., Mohamed, W.S., Ibrahim, A.H., Mohamed, H.M. (2024), The potential of new eco-friendly formulations in enhancing the protection of ceramic artifacts, *Journal of Cultural Heritage,* Vol. 67, pp. 404–413.

Mohamed, M. H. and Mohamed, S.W. (2023), Improving the properties of gap-filling materials for pottery artifacts with nano silica and nano kaolinite polymeric nanocomposites, *Pigment & Resin Technology*, doi: 10.1108/PRT-03-2023-0024.

Oleari, C (2000) Calorimetria e Beni Culturali, istituto centrale di restauro progetto beni culturali - CNR, Society i Italian di Ottica e Photonica, Italia (chrome-extension://efaidnbmnnnibpcajpcglclefindmkaj/https://www.gruppodelcolore.org/wp-content/uploads/2018/10/Atti_full_00.pdf)

Sarikaya, M., et al., (2018). Characterization of moganite obtained from natural zeolite by ball milling. *American Journal of Engineering Research* (AJER), Vol. 7,1, pp. 230-234

Shimmin, S. and van Strien, P.J. *(2018). History of Work of and the Organization Psychology*. A Handbook of Work and Organizational Psychology: Volume 1: Introduction to Work and Organizational Psychology, pp. 71.

Sansonetti, A., et al., (2010). Colored grounds of gilt stucco surfaces as analyzed by a combined microscopic, spectroscopic and elemental analytical approach. *Analytical and bioanalytical chemistry*, Vol. 397, pp. 2667-2676.

Talreja, N., Chauhan, D., and Ashfaq, M. (2023) Photo-Antibacterial Activity of Two- Dimensional (2D)-Based Hybrid Materials: Effective Treatment Strategy for Controlling Bacterial Infection, *Antibiotics,* Vol. 12, p. 398.

Treccozzi, D. Pane, A. Sansonetti, A. and Catuogno, R. (2020), Gabinetto of Gilded Stucco in the Royal Palace of Portici, Naples (ITALY): Survey and Diagnosis for Conservation, The International Archives of the Photogrammetry, Remote Sensing and Spatial Information Sciences, Volume XLIV-M-1-2020, HERITAGE2020 (3DPast-RISK-Terra) International Conference, 9–12 September 2020, Valencia, Spain, pp. 427-438.

Wang, Z., Huo, Y., Fan, Y., Wu, R., Wu, H., Wang, F., Xu, X. (2018) Facile synthesis of carbon-rich g-C3N4 by copolymerization of urea and tetracyanoethylene for photocatalytic degradation of Orange II, *Journal of Photochemistry and Photobiology A: Chemistry*, Vol. 358, pp. 61-69.

Wang, Y., et al., (2006) Tribological and corrosion behaviors of Al2O3/polymer nanocomposite coatings. *Wear,* Vol. 260, No. 9, pp. 976-983.

Wang, N., et al., (2023) Polymer@SiO2 Core–Shell Composite Particles: Preparation and Application. *Coatings*, Vol. 13, No. 2, pp. 334.

Wang, Z., et al., (2018) Facile synthesis of carbon-rich g-C3N4 by copolymerization of urea and tetracyanoethylene for photocatalytic degradation of Orange II. *Journal of Photochemistry and Photobiology A: Chemistry,* Vol. 358, pp. 61-69.

Wang, T., Song, B. and Wang, L. (2020) A new filler for epoxy resin: Study on the properties of graphite carbon nitride (g-c3n4) reinforced epoxy resin composites. *Polymers*, Vol.12, No., pp. 76.

Wang, X., et al., (2009) Metal-containing carbon nitride compounds: a new functional organic–metal hybrid material. *Advanced Materials*, Vol. 21, No.16, pp. 1609-1612.

Xiang, Q., Yu, J., and Jaroniec, M. (2011), Preparation and enhanced visible-light photocatalytic H2-production activity of graphene/C3N4 composites, *The Journal of Physical Chemistry C,* Vol. 115, pp.7355-7363.

Zhang, C., et al., (2020) Selectively Functionalized Zeolite NaY Composite Materials for High-Efficiency Multiple Protection of Paper Relics. Industrial & Engineering Chemistry Research, American Chemical Society, Vol.59, No 24, pp.11196-11205, Article 11196

Zheng, Y., et al., (2016) Surface hydroxylation of graphitic carbon nitride: Enhanced visible light photocatalytic activity. *Materials Research Bulletin*, Vol.84, pp. 46-56.

Zia-ur-Rehman, M., Murtaza, G., Qayyum, M. F., Saqib M., and Akhtar, J. (2017) Salt affected Soils: Sources, Genesis and Management, In book: Soil Science Concepts and applications, Chapter: 9, University of Agriculture Faisalabad, Editors: M. Sabir, J. Akhtar, K. R. Hakeem, pp. 193-195.

Zhang, C., et al., (2021) One-Pot Exfoliation and Functionalization of Zeolite Nanosheets for Protection of Paper-Based Relics. *ACS Applied Nano Materials*, Vol. 4, No.10, pp. 10645-10656.